ACS Chemical Neuroscience

Research Article

pubs.acs.org/chemneuro

Deciphering the Lipid Architecture of the Rat Sciatic Nerve Using Imaging Mass Spectrometry

Roberto Fernández,[†] Víctor Carriel,[§] Sergio Lage,[†] Jone Garate,[†] Javier Díez-García,[∥] Begoña Ochoa,[‡] Begoña Castro,[∥] Miguel Alaminos,[§] and José A. Fernández*[,†]

[†]Department of Physical Chemistry, Faculty of Science and Technology, [‡]Department of Physiology, Faculty of Medicine and Dentistry, University of the Basque Country UPV/EHU, 48940 Leioa, Spain

[§]Tissue Engineering Group, Department of Histology, Faculty of Medicine, University of Granada, 18012 Granada, Spain

[∥]Histocell, S.L., Bizkaia Technology Park 800, 48160 Derio, Spain

Supporting Information

ABSTRACT: Knowledge on the normal structure and molecular composition of the peripheral nerves is essential to understand their pathophysiology and to select the regeneration strategies after injury. However, the precise lipid composition of the normal peripheral nerve is still poorly known. Here, we present the first study of distribution of individual lipids in the mature sciatic nerve of rats by imaging mass spectrometry. Both positive and negative ion modes were used to detect, identify and in situ map 166 molecular species of mainly glycerophospholipids, sphingomyelins, sulfatides, and diacyl and triacylglycerols. In parallel, lipid extracts were analyzed by LC-MS/MS to verify and complement the identification of lipids directly from the whole tissue. Three anatomical regions were clearly identified by its differential lipid composition: the nerve fibers, the connective tissue and the adipose tissue that surrounds the nerve. Unexpectedly, very little variety of phosphatidylcholine (PC) species was found, being by far PC 34:1 the most abundant species. Also, a rich composition on sulfatides was detected in fibers, probably due to the important role they play in the myelin cover around axons, as well as an abundance of storage lipids in the adipose and connective tissues. The database of lipids here presented for each region and for the whole sciatic nerve is a first step toward understanding the variety of the peripheral nerves' lipidome and its changes associated with different diseases and mechanical injuries.

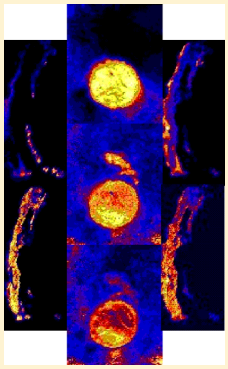

KEYWORDS: *Imaging mass spectrometry, lipidomics, peripheral nervous system*

The nerves and ganglia outside of the brain and spinal cord compose the peripheral nervous system (PNS), whose major function is to connect the central nervous system (CNS) to the organs and limbs, acting as a communication relay going back and forth between the brain and the extremities.

Peripheral nerves consist of a functional parenchyma, mainly, the nerve fibers formed by the axons and the surrounding Schwann cells, and a stroma composed by a specialized connective tissue organized in epineurial, perineurial and endoneurial layers.[1] The most external layer, epineurium, is usually rich in adipose tissue. The rat sciatic nerve is a mixed sensory-motor nerve consisting of one single fascicle corresponding to the fusion of the L4 and L5 spinal nerves,[2] which splits distally into two fascicles. The Schwann cells can interact with a single axon forming a myelinated nerve fiber or a single Schwann cell can interact with several axons forming unmyelinated nerve fibers. Previous reports demonstrated that the sciatic nerve is composed of 6% myelinated motor axons, 23% myelinated sensory axons, 48% unmyelinated sensory axons, and 23% unmyelinated sympathetic axons.[3]

Several diseases and mechanical injuries can damage the structure of nerves and their axons, which correlates with the severity of the resulting functional impairment. In fact, peripheral nerve injuries are frequent lesions that affect around 100 000 patients in the United States and Europe annually, which unless treated can cause long-term morbidity.[4] Following a structural disruption, the peripheral nerve has intrinsic capability to partially regenerate its components, and surgical repair may have variable success rates. In order to properly evaluate the regeneration process, it is necessary to identify the lipid composition and distribution in normal nerves. However, the exact lipid composition of these lipid-rich organs is not well-known.

Lipids are not directly genetically encoded. They are a family of hydrophobic and amphiphilic molecules that have evolved to perform a wide variety of structural, metabolic and regulatory functions. In mammals, the lipid family is remarkably diverse, comprising thousands of individual species, the lipidome, whose individual function is far from being elucidated. Lipid metabolism is very complex and is strictly regulated at different layers, including its spatial distribution in cells, tissues and whole body. Despite such regulation, disruption of lipid homeostasis occurs frequently, often related with the appearance and progression of common diseases, including Alzheimer's

Received: January 8, 2016
Accepted: April 4, 2016
Published: April 4, 2016

DOI: 10.1021/acschemneuro.6b00010
ACS Chem. Neurosci. 2016, 7, 624−632

disease,[5,6] Parkinson' disease,[6] cancer,[7] cardiovascular disease,[8] and metabolic disorders such nonalcoholic fatty liver.[9] Lipid concentration also varies due to traumatic injuries, as was recently demonstrated in ischemia models[10,11] and in traumatic brain injury.[12] Furthermore, several studies correlated changes in the lipid composition of nerves with diseases such as chronic pain,[13] alloxan-induced diabetes,[14] in patients with Refsum's disease[15] or in dysmyelinating trembler mice,[16] but also in regenerating sciatic nerves.[17]

Thus, changes in the lipidome may be good indicators of the severity of a lesion and of the regeneration of injured peripheral nerves. Likewise, it may be possible to evaluate the efficacy of therapeutic interventions directed to promote the regeneration of nerves, by observing the changes in their lipid composition. Such approaches require of more data and of a better understanding of the nerve's lipidome, because the information on the nerve's lipidome is scarce. To the best of our knowledge, the most recent studies on the subject are at least two decades old,[14,16,18−20] apart from the more recent work by Yost's group,[21,22] and a recent work on rodent's optic nerve,[23] both in the CNS. Here we extend such knowledge using MALDI-IMS (matrix assisted laser desorption/ionization-imaging mass spectrometry)[24−27] to comprehensively catalog and also to map the distribution of the most abundant lipid species in native, mature rat sciatic nerve. In order to detect the largest number of species, two matrices were used: 2-mercaptobenzothiazole[28] (MBT) both for positive- and negative-ion detection modes, and 1,5-diaminonapthalene[29] (DAN) to improve the number of species detected in negative-ion mode. In this way, more than 500 species (including $+H^+$, $+Na^+$, $+K^+$, $+[MBT + H]^+$, $-H^+$ adducts and redundant species detected both in positive and negative ion mode) were detected in a 200−2000 mass range, of which 203 (including adducts and both ionization modes) presented a univocal assignment and their distribution map is presented. These assignments were further confirmed by comparison with LC-MS/MS data from lipid extracts, obtaining the most accurate description of the lipidome of the peripheral nerve regions so far.

RESULTS AND DISCUSION

Figure 1 shows a sketch of a rat sciatic nerve. It consists of three types of tissues: the inner nerve fibers forming a single fascicle, the surrounding connective tissue layer and the external adipose tissue layer. The whole nerve is usually accompanied by adipocytes that populate the epineurium of the peripheral nerve and seem to have important implications in metabolic disease-associated peripheral neuropathies.[30] To characterize the lipid composition of all three kinds of tissue, both longitudinal and transversal sections were scanned using MALDI-IMS, both in positive- and negative-ion modes, to detect as many species as possible. In the upper part of Figure 1, the distribution of some representative species along a transversal section of a sciatic nerve is shown. Clearly, some species are distributed preferentially in the fibers, such as phosphatidylcholine (PC) 32:1+H^+, m/z = 732.554, while others are mainly located in the outer adipose tissue, as for example, PC 32:0+H^+ (m/z = 734.570). To conclude if there is a significant difference in lipid distribution between the regions of the sciatic nerve, a statistical analysis using a clustering algorithm was carried out. The algorithm groups the spectra according to their similarity, to form the number of clusters specified by the user. The top left image in Figure 1 shows the clusters formed by a k-means algorithm, setting the number of clusters to four. The area in

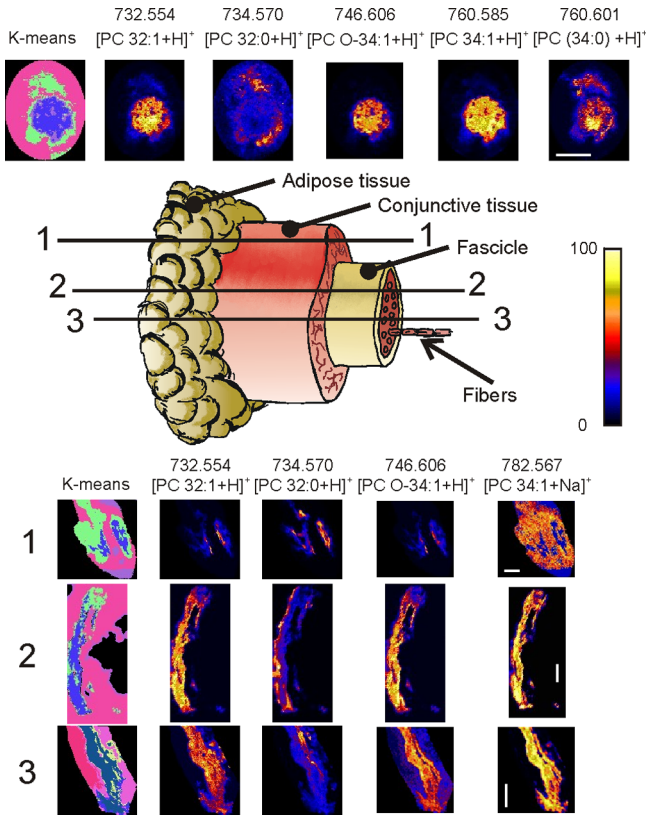

Figure 1. Lipid distribution along transversal and longitudinal sections of the mature rat sciatic nerve. Images were obtained using MBT as a matrix and positive detection mode. The statistical analysis (upper left image) shows three different areas: a nerve-fibers-rich region in blue, a region composed mainly of connective tissue (perineurium and the connective tissue associated with blood vessels into the endoneurium) in purple, and adipose-tissue-rich epineurium in green. The empty area surrounding the tissue corresponds to matrix and is colored in pink. The images were recorded at a pixel size of 25 μm. Scale bar = 1 mm.

pink corresponds to the spectra recorded outside the tissue section, which contain only peaks due to the MALDI matrix. The green areas very well match the distribution of adipose tissue around the nerve. These spectra are enriched in TG species (see Figures 2 and 3). The remaining spectra were classified into two groups: the one in blue in the figure follows the nerve fibers distribution, while the remaining purple areas correspond to the connective tissue: epineurium, perineurium, and intraneural connective tissue with blood vessels.

The same regions were also found when longitudinal sections were scanned (lower panels in Figure 1, numbered from 1 to 3), although depending on the height at which the section was taken, the relative contribution of each area to the image varied. Likewise, the relative contribution of each species also changed from transversal to longitudinal sections, as the percentage of each type of tissue was also variable. Consequently, the number and identity of the species found changed slightly from longitudinal to transversal sections, remarking the importance of scanning both sectioning types of samples to map lipids with precision.

It is clear from Figure 1 that the fibers present a characteristic lipid composition, different from the surrounding tissue. To emphasize such point, Figure 2 shows the average spectrum over each of the regions found by the statistical analysis, together with the image of each region for some example sections.

DOI: 10.1021/acschemneuro.6b00010
ACS Chem. Neurosci. 2016, 7, 624−632

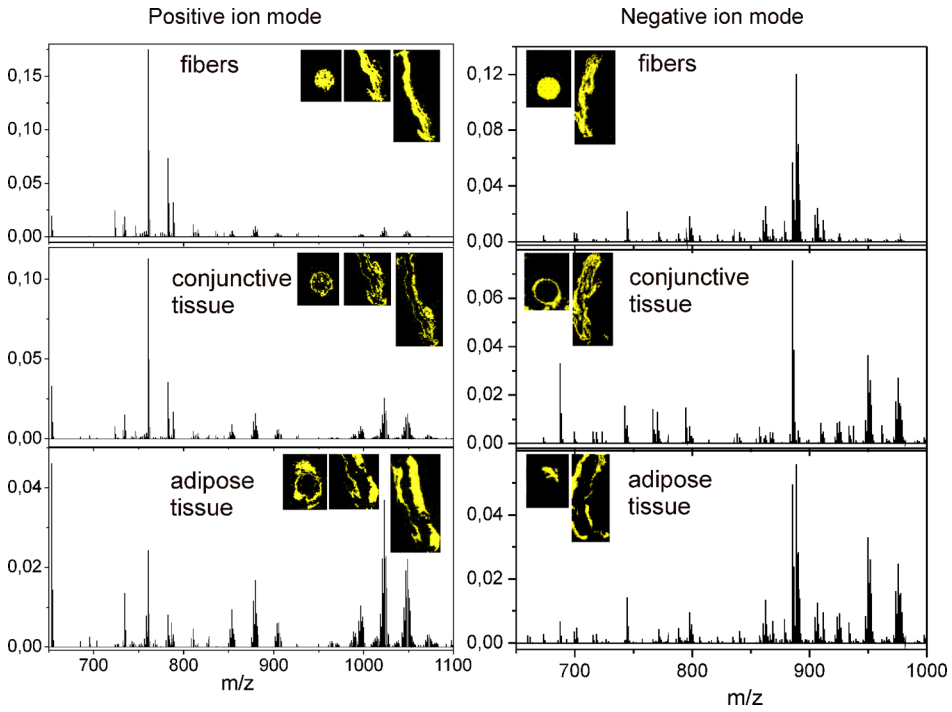

Figure 2. Average spectra over the three types of tissue found in sciatic nerve: fibers, connective tissue, and adipose tissue, recorded in positive (left) and negative (right) ion modes. Variation in the relative abundance of the lipids is clearly seen. Insets show clusters obtained using k-means that correspond to each kind of tissue in several example sections.

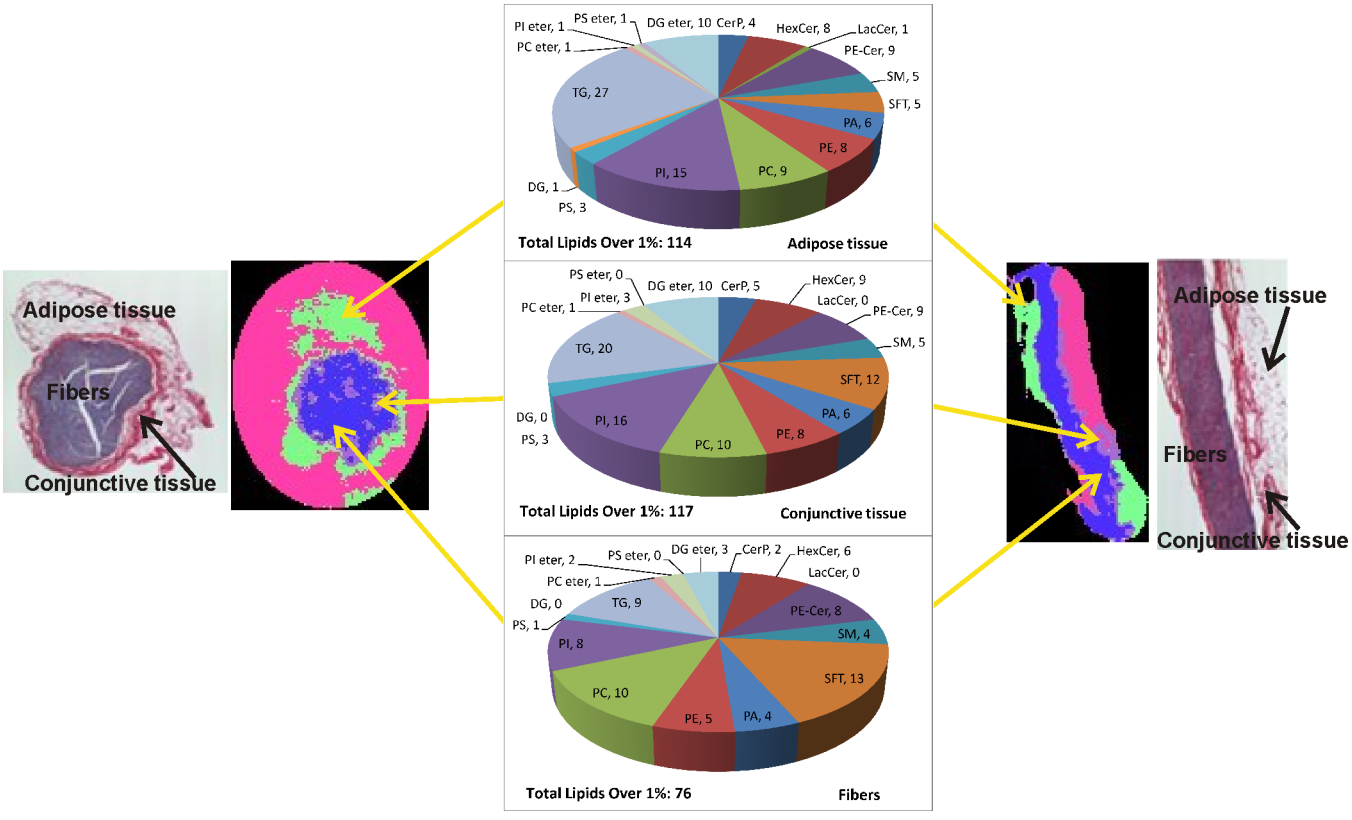

Figure 3. Total number of lipid species assigned in each region of the rat sciatic nerve. Two histological sections from different nerves are also shown for comparison.

Interestingly, the average mass spectrum over the fibers is dominated by a peak at m/z = 760.5851 that carries most of the intensity and that is assigned to PC 34:1+H$^+$, and by its Na adduct at m/z = 782.5689. The rest of the species are present in significantly lower abundance (Figures S1–S12 and Tables S1–S4). The average spectrum recorded in negative ion mode over

DOI: 10.1021/acschemneuro.6b00010
ACS Chem. Neurosci. 2016, 7, 624–632

region 1 shows a larger number of species, as it happens with other tissues.[31] Certainly, while in positive ion mode PC species dominate the spectrum (Figure S1), followed by sphingomielin (SM) and cerebrosides (Figure S2), phosphatidic acid (PA, Figure S3), triacylglycerol (TG, Figure S4), and diacylglycerol (DG, Figure S5) classes, the negative-ion mode usually allows a larger number of classes to be detected, including glycosilated acidic lipids: sulfatides (SFT, Figure S6), hexoxyl ceramides (HexCer, Figure S7), phosphatidylinositol (PI, Figure S8), Ceramide phosphatidylethanolamine (PE-Cer, Figure S9), phosphatidyletanolamine (PE, Figure S10), phosphatidylserine (PS, Figure S11), PA (Figure S12), and ceramide-1-phosphate (Cer-P, Figure S13). In this case, the spectrum is dominated by a peak at m/z = 888.624, assigned as SFT d18:1/24:1−H^-, which is mainly located in fibers (Figure 3), and a lower intensity peak at m/z = 885.550, which corresponds to PI 18:0/20:4−H^- and is regularly expressed across the three nerve regions (Figure 4). These two species are also the most abundant ones in the central nervous system, although the sulfatide is preferentially located in white matter.[27,32,33] Conversely, they are colocalized in the peripheral nerve. Both lipid classes seem to play roles related with the myelin. Thus, some studies point to the sulfatides with 2-hydroxylated and saturated long-chain fatty acids as myelin stabilizers,[34] while some authors point to some phosphorylated PIs as regulators of the homeostasis of myelin.[35]

On the other hand, the average spectrum recorded over connective tissue presents a reduction on the intensity of PC 16:0/18:1. It is worthy to note the gain in intensity of a group of peaks between m/z = 960−1100. Most of the species in such interval are TGs forming adducts with one MBT molecule and a proton. Such assignment is reinforced by the spectrum of the adipose tissue around the nerve, which is enriched in such species. Surprisingly, a large number of TG species were also found in negative ion mode both in connective and adipose tissues. Usually, such species are reported only in positive ion mode. May be their high abundance in the sample is the reason for their detection. So far, detection of TG species in negative-ion mode was only reported in human colon samples.[31] The assignment is also confirmed by the spectra recorded in positive ion mode and by the data from LC-MS/MS collected in Tables S1−S4.

Figure 3 shows the number of species of each lipid class present on each region of the tissue. The figure was created using all the species with relative abundance > 1% of the most abundant species in the average spectrum over each kind of tissue, and adding together the species detected in positive- and negative-ion modes. The lipid species detected from the rat sciatic nerve sections mainly consist of glycerolipids (LPC, PC, PE, PS, PI, PA, PG, TG, DG, and their ether species) and sphingolipids (SFT, SM, Cer-P, and PE-Cer) as well as glycosphingolipids (HexCer). Some other highly glycosylated lipids were also detected, but the identification could not be confirmed by LC-MS/MS, and therefore, they were excluded from the study. Clearly the fibers contain a reduced variety of lipids compared with the connective tissue, pointing to a more specialized function of the fibers. The small number of PE species detected by IMS (Table S1) may well be due to ion suppression by the presence of the PCs in the fibers, which lie in the same spectral region but that usually present stronger intensity. Certainly, the LC-MS/MS data show a significantly bigger number of PE species and a large abundance of PE-ether species. It must also be taken into account that only those species for which univocal assignment was found are presented here, and that several additional mass channels in the IMS spectra could be tentatively assigned as PEs, but they are not collected in Table S1 nor in the rest of the figures because we found alternative assignments for them that could not be ruled out.

Regarding the identity of the species, it is worthy to note that the detected PCs (Table S1 and Figure 4) present a very limited number of insaturations and that a reduced number of PC-ether species was detected, both directly from the tissue using IMS and from the extracts using LC-MS/MS. Such observation strongly contrasts with the observed DG species (Table S4 and Figure 4), which are mainly ether derivatives. These lipid species are produced in the peroxisomes as an intermediate step in the synthesis of PC and PE,[36] and therefore, one would expect a correlation between the number of DG-O and PC-O/PE-O. Unfortunately, the strong intensity of PC 34:1 hampers detection of PC/PE-ethers, that lie in the same spectral region but in a significantly lower abundance. Nevertheless, the results from the LC-MS/MS highlight the existence of such species in the nerve. It would be interesting to conduct future experiments to highlight the role played by these highly specialized lipids in the nerve. Some studies assign them antioxidant roles and functions related with the immune system,[37−39] and even with the existence and progression of cancer.[40−42] However, to establish a clear connection between the distributions observed in this work and such functions would require of in depth studies.

It is also remarkable the variety of SFT species detected in fibers and connective tissue (Figure S6 and Table S2). The presence in nerve fibers is probably because sulfatides are major components of Schwann cells myelin sheath[43] and to the abundance of this lipid class in the layers covering the axons (of which 29% are myelinated). The abundance of SFT in connective tissue might be explained by their functions in plasma membrane, as molecular clues for cell recognition, adhesion, and signaling,[44] in order to maintain the nerve fibers structure.

As one would expect, the adipose tissue is enriched in TGs and DGs (Figures 2, 4, S4, and S5), with PIs as the third most abundant class. Most peripheral nerves are partially surrounded by this type of tissue,[45] whose primary function might be mechanical protection. However, Verheijen and colleagues[30] demonstrated a crucial role of these lipids as energy sources in mature peripheral nerve function, with important implications for understanding peripheral neuropathies. During peripheral nerve development, transcription of a large number of genes involved in storage lipid metabolism is acutely activated only in mature peripheral nerve once myelination is complete.[30] Most of them are expressed in the adipocytes populating the epineurium but some in the endoneurium.[30] Certainly, the adipose tissue detected in the samples is associated with the epineurial connective layer surrounding the nerve. The presence of certain amounts of adipose tissue around the nerve has also been confirmed by the histological analysis of nerve samples (Figures 2−4). The lipid (TG) distribution of this peripheral adipose tissue was different from that of the connective tissue and the nerve fibers, suggesting area-specific biological functions and supporting the metabolic role of this adipose tissue.

Several additional lipid classes were also found. Among them, the most important ones are cerebrosides and gangliosides. However, they are not collected in Figure 4 or in Tables S1−S4 because assignment of such species is not straightforward without running MS/MS experiments, due to the extensive fragmentation patterns that they usually exhibit.[12,46−49] More complex lipids

DOI: 10.1021/acschemneuro.6b00010
ACS Chem. Neurosci. 2016, 7, 624−632

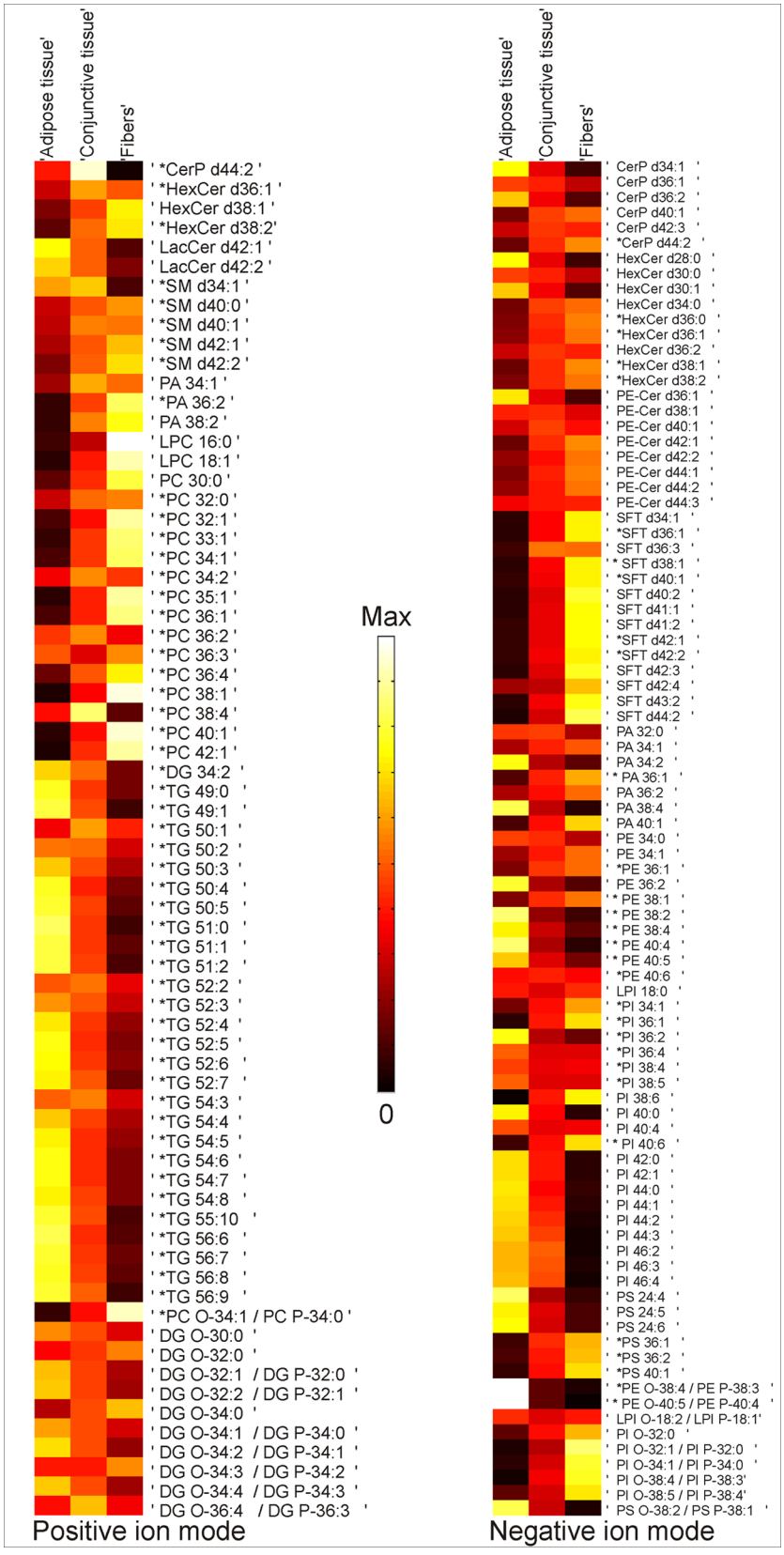

Figure 4. Heat map with the distribution of the detected lipid species in the three regions of the sciatic nerve detected in positive-ion mode (left) and negative-ion mode (right). The asterisks denote the species also detected by LC-MS/MS (see Tables S1−S4).

were also detected, such as penta- and hexa-acetyl-galactosyl ceramides (m/z = 1060.710, 1058.694, and 1032.679), which were previously detected in cerebrospinal fluid.[50]

Comparison with Literature. Previous studies on the lipidome of peripheral nerves are scarce and mainly related with changes on the relative abundance of lipid classes in the context

DOI: 10.1021/acschemneuro.6b00010
ACS Chem. Neurosci. 2016, 7, 624−632

of a given disease. Nevertheless, all the studies agree on several points: (1) the most abundant fatty acids are 16:0, 18:0, and 18:1; (2) there is little insaturation in the lipid composition; (3) after cholesterol, PC and PE are the most abundant lipid classes. Such observations are in good agreement with the results from the present study apart from the abundance of PEs, but the disagreement on that point may be due to the detectability of such species in tissues using MALDI-IMS. A remarkable difference in lipid composition between nerve fibers and connective tissue comes from the proportion of PC, which is higher in the axon-containing areas (Figure 4). On the other hand, PS and PI, are slightly decreased in nerve fibers that together with the PC difference may point to a higher total membrane content with less cell signaling function, which may correlate with the fundamental electrical isolator function of myelin.

Peripheral nerves contain axon bundles that convey sensory and motor information to connect central nervous system and target organs, and Schwann cells that generate a sheath of myelin that wraps part of the axons. The speed and precision of neurotransmission in axons depends on the nature of the information carried and is modulated by the thickness of myelin. Hence, myelin is a tightly organized and highly ordered membrane structure composed of high levels of saturated long chain lipids and is enriched in glycosphingolipids (mostly, galactosylceramides and sulfatides) and cholesterol that behaves as an electrical insulator. PE is a lipid class that is found in the inner leaflet of the cell membrane and that due to its molecular structure is related to the curvature of membrane monolayers[51] and therefore associated with myelin composition.[52] PS is another lipid class present in the inner leaflet of the cell membrane whose translocation to the outer membrane has been identified as molecular marker of early programmed cell death.[53] Our analysis revealed that different species of PE, 34:1, 36:1, and 38:1, colocalized with a high degree of overlapping as other members of PS family did (Figure 4), probably due to their metabolic relationship. Certainly, PE and PI are interconverted by the enzyme phosphatidylserine synthase 2.

In summary, IMS allowed us to identify the most important lipids that are present in the sciatic nerve and, more importantly, to determine the lipid distribution at each histological area of the nerve by using a straightforward scanning method. Once the lipidome of the native peripheral nerve has been described, this method could be very useful to determine the lipid distribution of nerves affected by different conditions and during nerve regeneration. These analyses will allow researchers to shed light on specific lipid-related mechanisms associated with disease and regeneration of peripheral nerve. Our groups are currently working in such tasks.

METHODS

Samples. Four adult healthy male Wistar rats kept at the animal facilities of the University Hospital *Virgen de las Nieves* of Granada (Spain) were deeply anesthetized using ketamine and acepromazin and perfused with paraformaldehyde. Both sciatic nerves from each rat were surgically excised including the parenchyma and stromal layers. Surgical manipulation of the nerve was minimized to prevent damaging its internal fibers arrangement. Nerves were then embedded in OCT compound, and 6 μm thick cryosections were obtained. This work was approved by the research and ethics committee for animal research of the University of Granada, Spain.

MALDI-IMS Analysis. In order to determine the lipid composition of the different histological areas of the sciatic nerve, nine longitudinal sections and two transversal sections were scanned using in positive-ion mode, while four longitudinal sections and four transversal sections were scanned in negative-ion mode. The procedure followed for matrix deposition can be found somewere.[41] Briefly, a glass sublimator (Ace Glass 8023) was used to deposit a uniform layer of matrix over the tissue sections. The whole process took ~10 min, during which the sections were under soft vacuum. For some of the samples, a matrix recrystallization was also performed, using a Petri glass dish and methanol (see ref 41 for details), which largely improved lipid signal, but that resulted in a loss of spatial resolution. All the samples were scanned in an LTQ-Orbitrap XL (ThermoFisher), equipped with an N_2 laser (100 μJ max power, elliptical spot, small axis 35−40 μm, large axis 166−170 μm, 60 Hz repetition rate),[31] using the orbitrap analyzer at maximum mass resolution (100,000 at m/z = 400 Da), while the spacing between spectra (spatial resolution) was varied between 10 and 100 μm, looking for a compromise between achieving the maximum resolution with a reasonable acquisition time. Finally, most of the samples were scanned at 25−50 μm. At least 20 shots grouped in two microscans were averaged to build the final mass spectrum of each point.

In order to correlate the lipid profile with the histological localization of the myelin and connective tissue, some peripheral nerve sections were prepared by tissue fixation in 4% buffered formalin, embedded in paraffin and sectioned at 5 μm of thickness, followed by staining using the MCOLL histochemical method.[54]

Data analysis was performed using dedicated software (MSIAnalyst, NorayBioinformatics S. L.). A detailed description of the procedure can be found in ref 41. In summary, after peak smoothing using the Savitzky−Golay algorithm,[55] the size of the data was reduced by selecting peaks through the Simple Peak Finding method[56] and by eliminating all the peaks whose intensity was lower than the 0.5% of the strongest peak on the spectrum. Then, the spectra were normalized using a total ion current algorithm[57] and aligned using the Xiong method.[58] During graphical representation, no interpolation or smoothing algorithms or any denoizing procedure was used, always trying to maintain the original aspect of the data. Statistical analysis was carried out using PCA (principal component analysis)[59] and k-means,[60] a clustering procedure, that takes into account all the mass-channels in the spectrum that survived the parsing stage. The k-means procedure showed a significantly better performance and therefore the results from the PCA analysis were not presented here.

Lipid identification in MALDI-IMS experiments was based on a direct comparison between the value of the m/z and the lipids in the software's lipid database (>33 000 species plus their adducts) and with those in the lipid maps database (www.lipidmaps.org). When multiple candidates were found for a given m/z, a further reduction was carried out by comparison with the data from LC-MS/MS. Mass accuracy was always better than 5 ppm and it was typically better than 3 ppm in the individual spectra. Data in Table S5 show larger deviations because the m/z are obtained from the average spectra, after aligning using the above-mentioned algorithm.

Lipid Extraction from Sciatic Nerves and UHPLC-MS/MS Conditions. Six segments of sciatic nerves were washed twice in ice cold PBS (phosphate buffer saline), after which they were weighed and homogenized on ice in 5 volumes of PBS with 10 bursts of 30 s on-and-off using a Polytron homogenizer (Kinematika, Switzerland). The homogenates were randomly pooled to generate two samples containing approximately 100 mg of sciatic nerve tissue in origin and transferred into glass tubes. Lipids were thoroughly extracted from the resulting homogenate pools (~3−4 mg protein) following the Bligh and Dyer procedure[61,62] and dried in a Savant SpeedVac concentrator (Thermo Scientific, Rockford, IL). Protein was estimated by the bicinconinic acid (BCA) protein assay (Thermo Scientific). Prior analysis, the lipid extracts were dissolved in a mixture of DCM/MeOH (2:1, v/v).

The liquid chromatography-tandem mass spectrometer consisted of a Synapt G2 HDMS (Waters, Milford, MA), operated in positive and negative electrospray ionization mode. Analytical column was a 100 mm × 2.1 mm i.d., 1.8 μm C8 Acquity UPLC HSS T3 (Waters). The mobile phase A was AcN/H_2O (40:60, v/v) and mobile phase B was AcN/isopropanol (10:90, v/v). Both eluents contained 10 mM NH4AcO as a buffering additive. A gradient was programmed as

DOI: 10.1021/acschemneuro.6b00010
ACS Chem. Neurosci. 2016, 7, 624−632

follows: from 0 to 10 min, 40 to 100% B in a linear mode, from 10 to 11, hold at 100% B, and re-equilibrate from 11 to 13 min at 0% B. The flow rate was 500 μL/min. The column was held at 65 °C. More detailed description of the spectrometer settings may be found in ref 41. Identification of the compounds was based on the accurate mass measurement with an error < 5 ppm, their LC retention time, and the fragmentation data, with the aid of SimLipid (Premier Biosoft).

■ ASSOCIATED CONTENT

Supporting Information

The Supporting Information is available free of charge on the ACS Publications website at DOI: 10.1021/acschemneuro.6b00010.

Tables with the identified lipids and graphics with their relative abundance in each kind of tissue (PDF)

■ AUTHOR INFORMATION

Corresponding Author

*Mailing address: CD1.S1.10, Departamento de Química Física, Facultad de Ciencia y Tecnología, Universidad del País Vasco (UPV/EHU), Barrio Sarriena s/n, 48940 Leioa, Spain. E-mail: josea.fernandez@ehu.es. Phone: +34946015387. Fax: +34946013500.

Author Contributions

Roberto Fernández prepared the samples for imaging mass spectrometry and processed the data. Jone Garate and Sergio Lage worked out LC/MS lipid assignment and IMS assignments, Victor Carriel and Miguel Alaminos obtained the samples from the animals and did the sectioning, Javier Díez coordinated the work between laboratories and the shipment of the samples and together with Begoña Ochoa aided in extracting the biologically-relevant conclusions from the results. José A. Fernández coordinated the IMS work and the interaction between the labs. All the authors participated in the writing of the manuscript and approved the final version.

Funding

This study was supported by the Spanish Ministry of Economy and Competitiveness, Grant IPT-2011-074-900000 (INNPACTO program), cofinanced by *Fondo Europeo de Desarrollo Regional* (FEDER). J.G. thanks the UPV/EHU for a predoctoral fellowship.

Notes

The authors declare no competing financial interest.

■ ACKNOWLEDGMENTS

Technical and human support provided by the *Servicio de Lipidómica* of the SGIKER (UPV/EHU, MICINN, GV/EJ, ESF) is gratefully acknowledged.

■ ABBREVIATIONS

Cer, ceramide; Cer-P, ceramide-1-phosphate; CNS, central nervous system; DG, diacylglycerol; DG-O, diacylglycerol ether; DAN, 2,5-diaminonaphtalene; MBT, 2-mercaptobenzothiazole; PA, phosphatidic acid; PC, phophatidylcholine; PC-O, phosphatidylcholine ether; PE, phosphatidylethanolamine; PE-Cer, Ceramide phosphatidylethanolamine; PI, phosphatidylinositol; PNS, peripheral nervous system; PS, phosphatidylserine; SFT, sulfatide; SM, sphingomyelin; S/N, signal-to-noise ratio; TG, triacylglycerol

■ REFERENCES

(1) Carriel, V., Alaminos, M., Garzón, I., Campos, A., and Cornelissen, M. (2014) Tissue engineering of the peripheral nervous system. *Expert Rev. Neurother. 14*, 301−318.

(2) Asato, F., Butler, M., Blomberg, H., and Gordh, T. (2000) Variation in rat sciatic nerve anatomy: Implications for a rat model of neuropathic pain. *J. Peripher. Nerv. Syst. 5*, 19−21.

(3) Schmalbruch, H. (1986) Fiber composition of the rat sciatic nerve. *Anat. Rec. 215*, 71−81.

(4) Kelsey, J. L., Praemer, A., Nelson, L. M., Felberg, A., and Rice, D. P. (1997) *Upper Extremity Disorders: Frequency, Impact, and Cost*, Churchill Livingstone, London.

(5) Jung, K. M., Astarita, G., Yasar, S., Vasilevko, V., Cribbs, D. H., Head, E., Cotman, C. W., and Piomelli, D. (2012) An amyloid + 42-dependent deficit in anandamide mobilization is associated with cognitive dysfunction in Alzheimer's disease. *Neurobiol. Aging 33*, 1522−1532.

(6) Valdes-Gonzalez, T., Goto-Inoue, N., Hirano, W., Ishiyama, H., Hayasaka, T., Setou, M., and Taki, T. (2011) New approach for glyco- and lipidomics- Molecular scanning of human brain gangliosides by TLC-Blot and MALDI-QIT-TOF MS. *J. Neurochem. 116*, 678−683.

(7) Zhang, F., and Du, G. (2012) Dysregulated lipid metabolism in cancer. *World J. Biol. Chem. 3*, 167−174.

(8) Tracy, R. P., and Tracy, P. B. (1997) New Views on the Relationship of Plasma Lipids to Cardiovascular Disease. *Circulation 95*, 1347−1348.

(9) Oresic, M., Hyotylainen, T., Kotronen, A., Gopalacharyulu, P., Nygren, H., Arola, J., Castillo, S., Mattila, I., Hakkarainen, A., Borra, R. J. H., Honka, M. J., Verrijken, A., Francque, S., Iozzo, P., Leivonen, M., Jaser, N., Juuti, A., Sorensen, T. I. A., Nuutila, P., Van Gaal, L., and Yki-Jarvinen, H. (2013) Prediction of non-alcoholic fatty-liver disease and liver fat content by serum molecular lipids. *Diabetologia 56*, 2266−2274.

(10) Hankin, J., Farias, S., Barkley, R., Heidenreich, K., Frey, L., Hamazaki, K., Kim, H. Y., and Murphy, R. (2011) MALDI Mass Spectrometric Imaging of Lipids in Rat Brain Injury Models. *J. Am. Soc. Mass Spectrom. 22*, 1014−1021.

(11) Koizumi, S., Yamamoto, S., Hayasaka, T., Konishi, Y., Yamaguchi-Okada, M., Goto-Inoue, N., Sugiura, Y., Setou, M., and Namba, H. (2010) Imaging Mass Spectrometry Revealed the Production of Lyso-Phosphatidylcholine in the Injured Ischemic Rat Brain. *Neuroscience 168*, 219−225.

(12) Colsch, B., and Woods, A. S. (2010) Localization and imaging of sialylated glycosphingolipids in brain tissue sections by MALDI mass spectrometry. *Glycobiology 20*, 661−667.

(13) Patti, G. J., Yanes, O., Shriver, L. P., Courade, J. P., Tautenhahn, R., Manchester, M., and Siuzdak, G. (2012) Metabolomics implicates altered sphingolipids in chronic pain of neuropathic origin. *Nat. Chem. Biol. 8*, 232−234.

(14) Pratt, J. H., Berry, J. F., Kaye, B., and Goetz, F. C. (1969) Lipid Class and Fatty Acid Composition of Rat Brain and Sciatic Nerve in Alloxan Diabetes. *Diabetes 18*, 556−561.

(15) MacBrinn, M. C., and O'Brien, J. S. (1968) Lipid composition of the nervous system in Refsum's disease. *J. Lipid Res. 9*, 552−561.

(16) Larrouquère−Règnier, S., Boiron, F., Darriet, D., Cassagne, C., and Bourre, J. M. (1979) Lipid composition of sciatic nerve from dysmyelinating trembler mouse. *Neurosci. Lett. 15*, 135−139.

(17) Alberghina, M., Viola, M., Moschella, F., and Giuffrida, A. M. (1983) Myelination of regenerating sciatic nerve of the rat: Lipid components and synthesis of myelin lipids. *Neurochem. Res. 8*, 133−150.

(18) Fressinaud, C., Rigaud, M., and Vallat, J. M. (1986) Fatty Acid Composition of Endoneurium and Perineurium from Adult Rat Sciatic Nerve. *J. Neurochem. 46*, 1549−1554.

(19) Klein, F., and Mandel, P. (1976) Lipid composition of rat sciatic nerve. *Lipids 11*, 506−512.

(20) Oulton, M., and Mezei, C. (1973) Development changes in lipid composition of chick sciatic nerve myelin. *Lipids 8*, 235−238.

(21) Landgraf, R. R., Garrett, T. J., Prieto Conaway, M. C., Calcutt, N. A., Stacpoole, P. W., and Yost, R. A. (2011) Considerations for quantification of lipids in nerve tissue using matrix-assisted laser desorption/ionization mass spectrometric imaging. *Rapid Commun. Mass Spectrom. 25*, 3178−3184.

DOI: 10.1021/acschemneuro.6b00010
ACS Chem. Neurosci. 2016, 7, 624−632

(22) Landgraf, R. R., Prieto Conaway, M. C., Garrett, T. J., Stacpoole, P. W., and Yost, R. A. (2009) Imaging of Lipids in Spinal Cord Using Intermediate Pressure Matrix-Assisted Laser Desorption-Linear Ion Trap/Orbitrap MS. *Anal. Chem. 81*, 8488−8495.
(23) Anderson, D. M. G., Mills, D., Spraggins, J., Lambert, W. S., Calkins, D. J., and Schey, K. L. (2013) High-resolution matrix-assisted laser desorption ionization-imaging mass spectrometry of lipids in rodent optic nerve tissue. *Mol. Vision 19*, 581−592.
(24) Fernandez, J. A., Ochoa, B., Fresnedo, O., Giralt, M. T., and Rodriguez-Puertas, R. (2011) Matrix-assisted laser desorption ionization imaging mass spectrometry in lipidomics. *Anal. Bioanal. Chem. 401*, 29−51.
(25) Caprioli, R., Stoeckli, M., and Chaurand, P. (1999) Image analysis of biological samples with matrix-assisted laser desorption ionization mass spectrometry. *Abs. Pap. Am. Chem. Soc. 217*, U138−U138.
(26) Caprioli, R. M., Farmer, T. B., Zhang, H. Y., and Stoeckli, M. (1997) Molecular imaging of biological samples by MALDI MS. *Abs. Pap. Am. Chem. Soc. 214*, 113-ANYL.
(27) Veloso, A., Astigarraga, E., Barreda-Gomez, G., Manuel, I., Ferrer, I., Giralt, M. T., Ochoa, B., Fresnedo, O., Rodriguez-Puertas, R., and Fernandez, J. A. (2011) Anatomical distribution of lipids in human brain cortex by imaging mass spectrometry. *J. Am. Soc. Mass Spectrom. 22*, 329−3338.
(28) Astigarraga, E., Barreda-Gomez, G., Lombardero, L., Fresnedo, O., Castano, F., Giralt, M. T., Ochoa, B., Rodriguez-Puertas, R., and Fernandez, J. A. (2008) Profiling and Imaging of Lipids on Brain and Liver Tissue by Matrix-Assisted Laser Desorption/Ionization Mass Spectrometry Using 2-Mercaptobenzothiazole as a Matrix. *Anal. Chem. 80*, 9105−9114.
(29) Thomas, A., Charbonneau, J. L., Fournaise, E., and Chaurand, P. (2012) Sublimation of New Matrix Candidates for High Spatial Resolution Imaging Mass Spectrometry of Lipids: Enhanced Information in Both Positive and Negative Polarities after 1,5-Diaminonapthalene Deposition. *Anal. Chem. 84*, 2048−2054.
(30) Verheijen, M. H. G., Chrast, R., Burrola, P., and Lemke, G. (2003) Local regulation of fat metabolism in peripheral nerves. *Genes Dev. 17*, 2450−2464.
(31) Garate, J., Fernandez, R., Lage, S., Bestard-Escalas, J., Lopez, D. H., Reigada, R., Khorrami, S., Ginard, D., Reyes, J., Amengual, I., Barcelo-Coblijn, G., and Fernandez, J. A. (2015) Imaging mass spectrometry increased resolution using 2-mercaptobenzothiazole and 2,5-diaminonaphtalene matrices: application to lipid distribution in human colon. *Anal. Bioanal. Chem. 407*, 4697−4708.
(32) Girod, M., Shi, Y. Z., Cheng, J. X., and Cooks, R. G. (2010) Desorption Electrospray Ionization Imaging Mass Spectrometry of Lipids in Rat Spinal Cord. *J. Am. Soc. Mass Spectrom. 21*, 1177−1189.
(33) Veloso, A., Fernández, R., Astigarraga, E., Barreda-Gómez, G., Manuel, I., Giralt, M. T., Ferrer, I., Ochoa, B., Rodríguez-Puertas, R., and Fernández, J. A. (2011) Distribution of lipids in human brain. *Anal. Bioanal. Chem. 401*, 89−101.
(34) Schmitt, S., Cantuti Castelvetri, L., and Simons, M. (2015) Metabolism and functions of lipids in myelin. *Biochim. Biophys. Acta, Mol. Cell Biol. Lipids 1851*, 999−1005.
(35) Aggarwal, S., Yurlova, L., and Simons, M. (2011) Central nervous system myelin: structure, synthesis and assembly. *Trends Cell Biol. 21*, 585−593.
(36) Wallner, S., and Schmitz, G. (2011) Plasmalogens the neglected regulatory and scavenging lipid species. *Chem. Phys. Lipids 164*, 573−589.
(37) Zoeller, R. A., Lake, A. C., Nagan, N., Gaposchkin, D. P., Legner, M. A., and Lieberthal, W. (1999) Plasmalogens as endogenous antioxidants: somatic cell mutants reveal the importance of the vinyl ether. *Biochem. J. 338*, 769−776.
(38) Brites, P., Waterham, H. R., and Wanders, R. J. A. (2004) Functions and biosynthesis of plasmalogens in health and disease. *Biochim. Biophys. Acta, Mol. Cell Biol. Lipids 1636*, 219−231.
(39) Braverman, N. E., and Moser, A. B. (2012) Functions of plasmalogen lipids in health and disease. *Biochim. Biophys. Acta, Mol. Basis Dis. 1822*, 1442−1452.
(40) Smith, R., Lespi, P., Di Luca, M., Bustos, C., Marra, F., de Alaniz, M. T., and Marra, C. (2008) A Reliable Biomarker Derived from Plasmalogens to Evaluate Malignancy and Metastatic Capacity of Human Cancers. *Lipids 43*, 79−89.
(41) (a) Fernández, R., Lage, S., Abad-García, B., Barceló-Coblijn, G., Terés, S., López, D. H., Guardiola-Serrano, F., Martín, M. L., Escribá, P. V., and Fernández, J. A. (2014) Analysis of the Lipidome of Xenografts Using MALDI-IMS and UHPLC-ESI-QTOF. *J. Am. Soc. Mass Spectrom. 25*, 1237−1246. (b) Hankin, J. A., Barkley, R. M., and Murphy, R. C. (2007) Sublimation as a method of matrix application for mass spectrometric imaging. *J. Am. Soc. Mass Spectrom. 18*, 1646−1652.
(42) Fernández, R., Garate, J., Lage, S., Terés, S., Higuera, M., Bestard-Escalas, J., López, D., Guardiola-Serrano, F., Escribá, P., Barceló-Coblijn, G., and Fernández, J. (2016) Identification of Biomarkers of Necrosis in Xenografts Using Imaging Mass Spectrometry. *J. Am. Soc. Mass Spectrom. 27*, 244−254.
(43) Quattrini, A., Corbo, M., Dhaliwal, S. K., Sadiq, S. A., Lugaresi, A., Oliveira, A., Uncini, A., Abouzahr, K., Miller, J. R., Lewis, L., Estes, D., Cardo, L., Hays, A. P., and Latov, N. (1992) Anti-Sulfatide Antibodies in Neurological Disease - Binding to Rat Dorsal-Root Ganglia Neurons. *J. Neurol. Sci. 112*, 152−159.
(44) Hakomori, S., and Igarashi, Y. (1995) Functional-Role of Glycosphingolipids in Cell Recognition and Signaling. *J. Biochem. 118*, 1091−1103.
(45) Ortiz-Hidalgo, C., and Weller, R. O. (2012) In *Peripheral Nervous System* (Kluwer, W., Ed.), 4th ed., Lippincott Williams & Wilkins, Philadelphia.
(46) Chan, K., Lanthier, P., Liu, X., Sandhu, J. K., Stanimirovic, D., and Li, J. J. (2009) MALDI mass spectrometry imaging of gangliosides in mouse brain using ionic liquid matrix. *Anal. Chim. Acta 639*, 57−61.
(47) Goto-Inoue, N., Hayasaka, T., Taki, T., Gonzalez, T. V., and Setou, M. (2009) A new lipidomics approach by thin-layer chromatography-blot-matrix-assisted laser desorption/ionization imaging mass spectrometry for analyzing detailed patterns of phospholipid molecular species. *J. Chromatography A 1216*, 7096−7101.
(48) Wang, H. Y. J., Post, S. N. J. J., and Woods, A. S. (2008) A minimalist approach to MALDI imaging of glycerophospholipids and sphingolipids in rat brain sections. *Int. J. Mass Spectrom. 278*, 143−149.
(49) Jackson, S. N., Ugarov, M., Post, J. D., Egan, T., Langlais, D., Schultz, J. A., and Woods, A. S. (2008) A Study of Phospholipids by Ion Mobility TOFMS. *J. Am. Soc. Mass Spectrom. 19*, 1655−1662.
(50) Podbielska, M., Dasgupta, S., Levery, S. B., Tourtellotte, W. W., Annuk, H., Moran, A. P., and Hogan, E. L. (2010) Novel myelin penta- and hexa-acetyl-galactosyl-ceramides: structural characterization and immunoreactivity in cerebrospinal fluid. *J. Lipid Res. 51*, 1394−1406.
(51) Chernomordik, L. V., and Zimmerberg, J. (1995) Bending membranes to the task: structural intermediates in bilayer fusion. *Curr. Opin. Struct. Biol. 5*, 541−547.
(52) Farooqui, A. A., Farooqui, T., and Horrocks, L. A. (2002) Molecular species of phospholipids during brain development. Their occurrence, separation and roles. In *Brain Lipids and Disorders in Biological Psychiatry* (Skinner, E. R., Ed.), pp 147−158, Elservier Science B. V., Amsterdam.
(53) Vermes, I., Haanen, C., Steffens-Nakken, H., and Reutellingsperger, C. (1995) A novel assay for apoptosis Flow cytometric detection of phosphatidylserine expression on early apoptotic cells using fluorescein labelled Annexin V. *J. Immunol. Methods 184*, 39−51.
(54) Carriel, V., Garzon, I., Alaminos, M., and Campos, A. (2011) Evaluation of myelin sheath and collagen reorganization pattern in a model of peripheral nerve regeneration using an integrated histochemical approach. *Histochem. Cell Biol. 136*, 709−717.
(55) Savitzky, A., and Golay, M. J. E. (1964) Smoothing and Differentiation of Data by Simplified Least Squares Procedures. *Anal. Chem. 36*, 1627−1639.

DOI: 10.1021/acschemneuro.6b00010
ACS Chem. Neurosci. 2016, 7, 624−632

(56) Coombes, K. R., Fritsche, H. A., Clarke, C., Chen, J. n., Baggerly, K. A., Morris, J. S., Xiao, L. c., Hung, M. C., and Kuerer, H. M. (2003) Quality Control and Peak Finding for Proteomics Data Collected from Nipple Aspirate Fluid by Surface-Enhanced Laser Desorption and Ionization. *Clin. Chem. 49*, 1615−1623.
(57) Deininger, S. O., Cornett, D. S., Paape, R., Becker, M., Pineau, C., Rauser, S., Walch, A., and Wolski, E. (2011) Normalization in MALDI-TOF imaging datasets of proteins: practical considerations. *Anal. Bioanal. Chem. 401*, 167−181.
(58) Xiong, X. C., Fang, X., Ou, Y. Z., Jiang, Y., Huang, Z. J., and Zhang, Y. K. (2012) Artificial Neural Networks for Classification and Identification of Data of Biological Tissue Obtained by Mass-Spectrometry Imaging. *Chinese J. Anal Chem. 40*, 43−49.
(59) Wold, S., Esbensen, K., and Geladi, P. (1987) Principal Component Analysis. *Chemom. Intell. Lab. Syst. 2*, 37−52.
(60) Arthur, D., and Vassilvitskii, S. (2007) *k-means++: The advantages of careful seeding*, pp 1027−1035, Society for Industrial and Applied Mathematics, New Orleans, LA.
(61) Bligh, E. G., and Dyer, W. J. (1959) A Rapid Method of Total Lipid Extraction and Purification. *Can. J. Biochem. Physiol. 37*, 911−917.
(62) Palacios, L., Ochoa, B., José Gómez-Lechón, M., Vicente Castell, J., and Fresnedo, O. (2006) Overexpression of SND p102, a rat homologue of p100 coactivator, promotes the secretion of lipoprotein phospholipids in primary hepatocytes. *Biochim. Biophys. Acta, Mol. Cell Biol. Lipids 1761*, 698−708.

DOI: 10.1021/acschemneuro.6b00010
ACS Chem. Neurosci. 2016, 7, 624−632